Dense Polarized Positrons from Laser-Irradiated Foil Targets in the QED Regime

Huai-Hang Song,[1,3] Wei-Min Wang,[2,4,*] and Yu-Tong Li[1,3,5,†]

[1]Beijing National Laboratory for Condensed Matter Physics, Institute of Physics, Chinese Academy of Sciences, Beijing 100190, China

[2]Department of Physics and Beijing Key Laboratory of Opto-electronic Functional Materials and Micro-nano Devices, Renmin University of China, Beijing 100872, China

[3]School of Physical Sciences, University of Chinese Academy of Sciences, Beijing 100049, China

[4]Collaborative Innovation Center of IFSA, Shanghai Jiao Tong University, Shanghai 200240, China

[5]Songshan Lake Materials Laboratory, Dongguan, Guangdong 523808, China

(Received 14 December 2021; revised 13 May 2022; accepted 13 June 2022; published 11 July 2022)

Many works have shown that dense positrons can be effectively generated from laser-solid interactions in the strong-field quantum electrodynamics (QED) regime. Whether these positrons are polarized has not yet been reported, limiting their potential applications. Here, by polarized QED particle-in-cell simulations including electron-positron spin and photon polarization effects, we investigate a typical laser-solid setup that an ultraintense linearly polarized laser irradiates a foil target with micrometer-scale-length preplasmas. We find that once the positron yield becomes appreciable with the laser intensity exceeding 10^{24} W/cm^2, the positrons are obviously polarized. Around 30 nC positrons can acquire $>30\%$ polarization degree with a flux of 10^{12} sr^{-1}. The angle-dependent polarization is attributed to the asymmetrical laser fields that positrons undergo near the skin layer of overdense plasmas, where radiative spin flip and radiation reaction play significant roles. The polarization mechanism is robust and could generally appear in future 100-PW-class laser-solid experiments.

DOI: 10.1103/PhysRevLett.129.035001

Polarized positrons with a preferential orientation of spins can exhibit unique features in many areas, such as searching new physics beyond the standard model in International Linear Collider (ILC) [1,2] and probing spin phenomena at material surfaces [3,4]. Polarized electron-positron (e^-e^+) plasmas are believed to be ubiquitous in pulsar magnetospheres [5,6]. There are a few methods to generate high-energy polarized positrons. Ultrarelativistic positrons in tesla-level magnetic fields of storage rings can be polarized via radiative spin flip [7,8], but rather slowly. Alternatively, polarized positrons are usually produced via Bethe-Heitler (BH) process by hitting high-Z targets with circularly polarized γ photons [9,10] or prepolarized electrons [11]. These BH methods suffer low conversion efficiency of about 10^4 positrons (10^{-6} nC) per shot, and thus high repetitions are necessary to meet the high-charge or high-density requirements of ILC (3.2 nC) and laboratory astrophysics [12,13].

Much denser positrons can be efficiently generated from single-shot laser-matter interactions in the strong-field quantum electrodynamics (QED) regime [14–18]. This approach is becoming experimentally feasible with advances in high-intensity laser technologies [19]. Recently, 1.1×10^{23} W/cm^2 intensity has been realized by a 4-PW laser system [20], and higher-power laser facilities of 10-PW [21] to 100-PW [22–25] classes will be available. In such strong laser fields, γ photons can be radiated by electrons and in turn annihilate into e^-e^+ pairs via multiphoton Breit-Wheeler (BW) process [26]. For all-optical configurations of lasers colliding with unprepolarized multi-GeV electrons [27,28], polarized positrons are available if laser fields are asymmetric, such as elliptically polarized [29] or two-color linearly polarized [30] lasers. Limited by the charge of electron beams from laser wakefield accelerations, the corresponding positron yield is only 10^{-4} nC level. Furthermore, constructing such asymmetric strong laser fields is challenging due to low damage thresholds of optical devices [31]. Recent QED particle-in-cell (PIC) simulations have shown that impinging on stationary targets by lasers above 10 PW [32–37] is capable of generating dense and more than 10 nC positrons via self-sustained QED cascades. However, it remains unclear whether such positrons are polarized or not as the QED models being widely adopted in existing QED PIC codes [37–40] overlook polarization effects.

In this Letter, a polarized QED PIC code [41,42] including e^-e^+ spin and photon polarization effects is employed to clarify the questions. We numerically investigate a linearly polarized laser interaction with a solid foil target with micrometer-scale-length preplasmas, as depicted in Fig. 1(a). For laser intensities exceeding 10^{24} W/cm^2, substantial positrons are created primarily near the skin layer of solid-density plasmas, where the dominance of laser magnetic components is favorable for e^-e^+ creation. Then, positrons are quickly pushed into

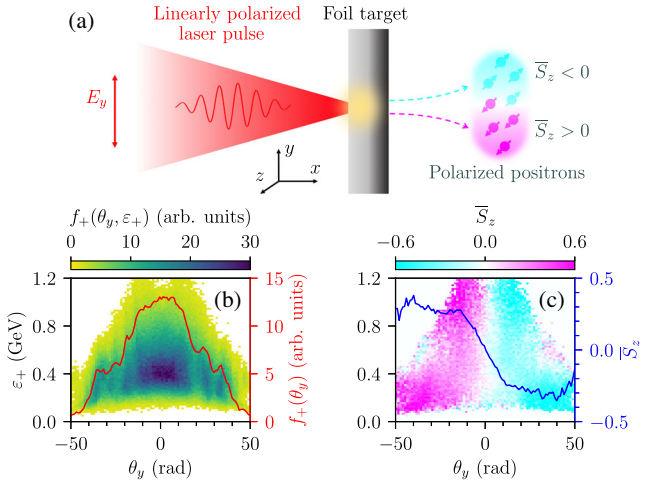

FIG. 1. (a) Schematic for generating polarized positrons in laser-solid interactions, where a linearly polarized laser pulse impinges on a foil target with micrometer-scale-length preplasmas. Positrons of two polarizations $\bar{S}_z > 0$ and $\bar{S}_z < 0$ are deflected along opposite angles $\theta_y < 0$ and $\theta_y > 0$, respectively, where $\theta_y = \arctan(p_y/|p_x|)$. (b) and (c) are distributions of positron number $f_+(\theta_y, \varepsilon_+)$ and polarization $\bar{S}_z$ versus θ_y and energy ε_+ at the end of interactions, where $f_+(\theta_y)$ and $\bar{S}_z$ versus θ_y are plotted by curves.

deeper plasmas and escape from the laser fields, causing them only to experience subcycle laser fields. In such asymmetric fields, positrons are split into two populations of opposite polarizations at different deflected angles. Above 30% polarization of around 30 nC positrons can be achieved and it can even reach 60% at some angles and energies. In future 100-PW laser-solid experiments even aiming at other applications [35,37,43], skin layers can be certainly formed and consequently, polarized positrons and electrons could be ubiquitous, indicating polarization effects should be considered.

Simulation setups.—We perform polarized QED PIC simulations to investigate positron polarizations sketched above with recently developed YUNIC [41,42] code. The strength of QED is characterized by the quantum invariant parameter $\chi_e = (|e|\hbar/m_e^3c^4)|F_{\mu\nu}p^\nu|$, where $F_{\mu\nu}$ is field tensor, p^ν is e^-e^+ four-momentum, $\hbar$ is reduced Planck constant, c is speed of light, and e and m_e are electron charge and mass. Two leading multiphoton QED processes of Compton scattering and BW pair production are implemented through the standard Monte Carlo algorithm [38–40], but including e^-e^+ spin and photon polarization effects [15,44–46]. Since mean axes are selected as quantization axes, spin vectors $\boldsymbol{S}$ of nonradiating electrons and positrons as well as Stokes vectors $\boldsymbol{\xi}$ of nondecaying photons also need to be updated [46]. More implementation details can be found from the Supplemental Material (SM) [47].

We first adopt one-dimensional (1D) PIC simulations to better get insight into the positron polarization mechanism with higher numerical resolutions, where the geometry is 1D while $\boldsymbol{S}$, $\boldsymbol{\xi}$ and particle momenta $\boldsymbol{p}$ remain fully three dimensional (3D). A laser pulse linearly polarized along the y direction is normally launched from the left boundary $x = 0$ at the initial time $t = 0$. The laser has a duration $\tau_0 = 20$ fs (FWHM of Gaussian temporal envelope), central wavelength $\lambda_0 = 1$ μm, and normalized amplitude $a_0 = |e|E_L/m_e c\omega_0 = 1500$ (peak intensity 3×10^{24} W/cm^2), where E_L and ω_0 are laser amplitude and frequency. An initially unpolarized and preionized carbon foil target of an electron density $n_0 = 530n_c$ is placed at $x = 9.75\lambda_0$ with a thickness $d = 0.5$ μm, where the critical density $n_c = m_e\omega_0^2/2\pi e^2 \approx 1.1 \times 10^{21}$ cm^{-3}. In the front of the foil target, there are preplasmas following an exponential density profile with a scale length $L = 1.5$ μm. The simulation domain $L_x = 20\lambda_0$, cell size $\Delta x = \lambda_0/96$, 500 electrons/C^{6+} ions per cell are taken. The laser cannot penetrate into the foil target through relativistic transparency because laser fields are strongly dissipated in front preplasmas via QED cascades [37].

Polarized positron properties.—By laser direct accelerations, some electrons from preplasmas quickly gain hundreds of mega-electron-volt energies to emit γ photons. Here, the boosted field strength in the electron rest frame can exceed the Schwinger limit to achieve $\chi_e \gtrsim 1$, entering the QED-dominated regime. By the end of interactions $t = 28T_0$, up to 94% laser energies are absorbed, with 63% transferred into γ photons, 18% into e^-e^+ pairs, and 13% into ions. If e^-e^+ spin and photon polarization effects are not considered, the pair yield is overestimated by about 7%, close to our recent PIC results with counterpropagating laser pulses [42].

Figures 1(b) and 1(c) illustrate that transversely polarized positrons are obtained and their polarizations are angle dependent. Positrons deflected along $\pm y$ directions are polarized along $\mp z$ directions. With the larger deflection angle $|\theta_y|$, positrons generally possess the higher polarization degree $|\bar{S}_z|$, which can reach 30% for $|\theta_y| > 20°$ [blue line in Fig. 1(c)]. More than 50% of total positrons acquire a 30% polarization through the angular selection. In addition, $|\bar{S}_z|$ also depends on positron energies, with higher values in lower-energy and higher-energy regions; it can reach 60% at some angles and energies, accounting for 1% positrons.

Polarization mechanism.—Positrons are mainly created near the plasma skin layer at the target front surface, where laser magnetic fields are dominated over electric fields [51] [Fig. 2(a)]. The magnetic-field-dominated regime (MFDR) favors QED processes, while the electric-field-dominated regime (EFDR) facilitates e^-e^+ accelerations [52,53], because magnetic fields are always approximately perpendicular to particle velocities, whereas electric fields are not. Considering that positrons are discretely produced with a period of half laser cycle, we will focus on positrons created at around $t = 21T_0$, as marked by the elliptical zone

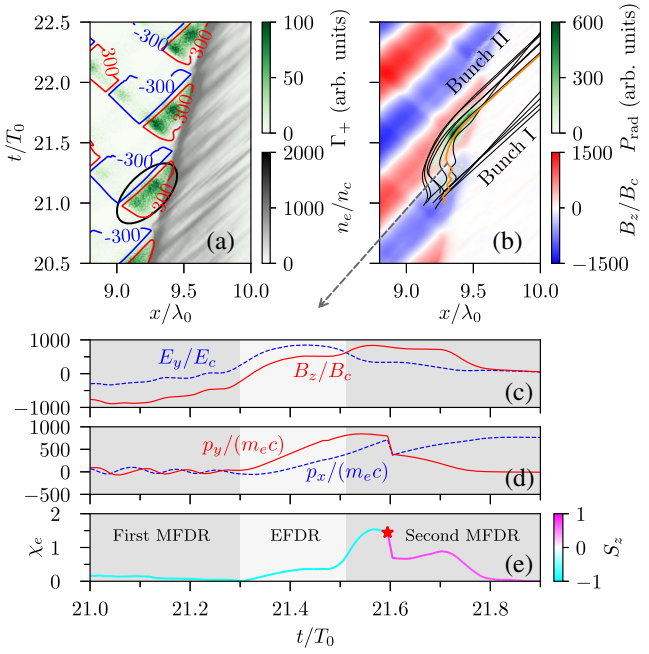

FIG. 2. (a) Spatiotemporal (x-t) evolution of electron density n_e and positron creation rate Γ_+, where Γ_+ represents positrons created per unit length and unit time. Contour lines of $|B_z/B_c| - |E_y/E_c| = 300$ (MFDR) and -300 (EFDR) are plotted, where $E_c(B_c) = m_e c\omega_0/|e|$. (b) Magnetic field B_z and radiation power $P_{\rm rad}$ of marked positrons created in the elliptical zone marked in (a). Several marked positrons are tracked, indicating they can be classified into two bunches, denoted as bunch I and bunch II. (c)–(e) Evolution of a typical bunch-II positron [the orange trajectory in (b)]: (c) experienced fields E_y and B_z, (d) momenta p_x and p_y, and (e) QED parameter χ_e and spin component S_z, where light-gray and dark-gray regions denote EFDR and MFDR, respectively, and the red star in (e) represents a strong radiation event.

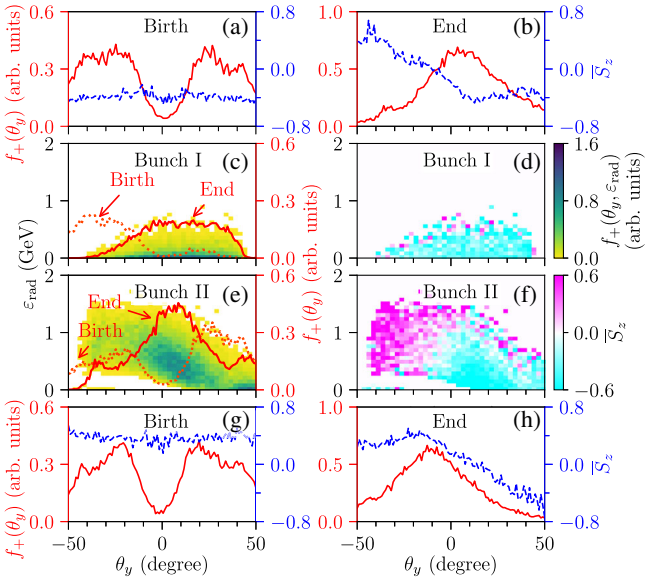

FIG. 3. (a)–(f) show positrons created in the negative half cycle [elliptical zone marked in Fig. 2(a)]; (g) and (h) are those in the next positive half cycle for comparison. The positron number $f_+(\theta_y)$ and polarization $\bar{S}_z$ versus the deflection angle θ_y [(a),(g)] at birth and [(b),(h)] at the end of interactions. [(c),(e)] $f_+(\theta_y, \varepsilon_{\rm rad})$ and [(d),(f)] $\bar{S}_z$ versus θ_y and $\varepsilon_{\rm rad}$ at the end of interactions for [(c),(d)] bunch I and [(e),(f)] bunch II, where $\varepsilon_{\rm rad}$ is the total radiation energy per positron. $f_+(\theta_y)$ versus θ_y at birth and at the end of interactions are also plotted by curves in (c) and (e).

in Fig. 2(a). The obtained results can be analogously extended to other half cycles.

In the marked zone, positrons are created in a negative half cycle of $B_z < 0$, causing the polarization to acquire a negative value $\bar{S}_z \approx -0.4$ [Fig. 3(a)]. This is because positron spins at birth have higher probabilities to be parallel to the magnetic field direction $\boldsymbol{\zeta} \equiv \boldsymbol{B}'/|\boldsymbol{B}'|$ in their respective rest frames as their parent γ photons of high energies are weakly linearly polarized in the x-y plane (Fig. S6 in SM). Here, $\boldsymbol{B}' \approx \gamma_e[\boldsymbol{B} - \boldsymbol{\beta} \times \boldsymbol{E} - \boldsymbol{\beta}(\boldsymbol{\beta} \cdot \boldsymbol{B})]$, $\boldsymbol{\beta}$ denotes unit vector along the positron velocity, and γ_e is the relativistic factor. Considering that $\boldsymbol{\beta}$ is directed in the x-y plane, $\boldsymbol{\zeta} \approx (0, 0, B_z/|B_z|)$ can be obtained in the MFDR, hence $\bar{S}_z$ of newly created positrons has the same sign with B_z. From Fig. 3(a), the positron number and polarization at birth are both essentially symmetrical with respect to $\theta_y = 0$. Similarly, positrons created in adjacent positive half cycles also exhibit similar distributions, but with $\bar{S}_z > 0$ due to $B_z > 0$ [Fig. 3(g)]. Thus, positron polarizations at birth in positive and negative half cycles would be canceled out. However, asymmetric subcycle laser fields that positrons experience later can break the polarization symmetry and cause the angle-dependent polarization. In all half cycles at the end of interactions, $\bar{S}_z > 0$ at $\theta_y < 0$ and $\bar{S}_z < 0$ at $\theta_y > 0$ are achieved [Figs. 3(b) and 3(h)], where spin flip and radiation reaction play significant roles.

The marked positrons are pushed forward after being created, and gradually divide into bunch I and bunch II [Fig. 2(b)]. Two bunches successively escape laser fields from two adjacent half cycles, with the relative number $N_+^{\rm I} : N_+^{\rm II} \approx 3:5$. Only experiencing the first MFDR where they are created, bunch-I positrons are quickly pushed forward into deeper plasmas, as their initial negative momenta $p_y < 0$ [red-dotted line in Fig. 3(c)] lead to strong forward Lorentz forces, i.e., $\beta_y B_z$ along the $+x$ direction. Without undergoing any EFDR for accelerations, bunch-I positrons are generally less energetic and weakly radiating [Fig. 3(c)], hence almost retaining the initial negative polarization [Fig. 3(d)]. By contrast, bunch-II positrons travel through an EFDR to obtain higher energies and then through the second MFDR for strong radiation [Fig. 3(e) and also $P_{\rm rad}$ plot in Fig. 2(b)]. Because of quantum stochasticity, spins of only a fraction of bunch-II positrons can flip parallel to $\boldsymbol{\zeta}$ and achieve an opposite polarization of $\bar{S}_z > 0$ [Fig. 3(f)] as $B_z > 0$ in the second MFDR.

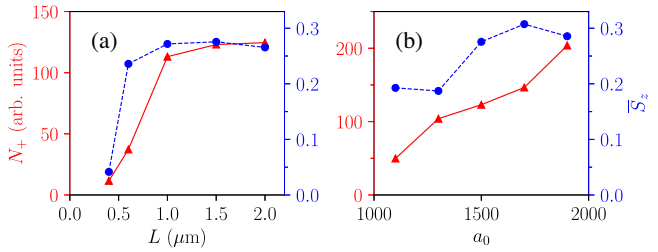

FIG. 4. The positron yield N_+ (solid triangle) and polarization $\bar{S}_z$ (dashed circle) at $\theta_y > 20^\circ$ versus (a) the preplasma scale length L and (b) laser amplitude a_0, respectively, where we take $a_0 = 1500$ in (a) and $L = 1.5$ μm in (b). Other parameters are the same as Fig. 1.

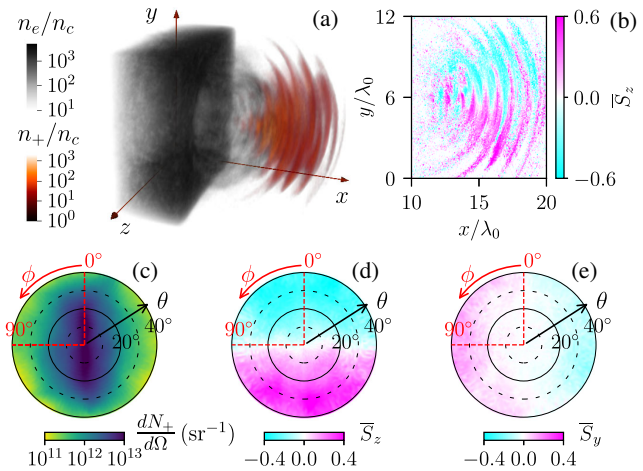

FIG. 5. 3D PIC simulation results. (a) Densities of the electron n_e and positron n_+. (b) Central slice of positron polarization $\bar{S}_z$ in the x-y plane. (c) Positron flux and two positron polarization components (d) $\bar{S}_z$ and (e) $\bar{S}_y$ versus the polar angle θ and azimuthal angle ϕ, where the laser is polarized along $\phi = 0, 180^\circ$ and propagates along $\theta = 0$.

Figures 3(e) and 3(f) show that part bunch-II positrons with final $\bar{S}_z > 0$ mainly appear at $\theta_y < 0$. This is caused by strong radiation reaction and can be explained by tracking a typical bunch-II positron [Figs. 2(c)–2(e)]. Under Lorentz force and radiation reaction, its transverse momentum p_y can be approximated as $p_y \approx p_{y0} + \int dt\{|e|(E_y - \beta_x B_z) - [p_y/(\gamma_e m_e c^2)]P_{\rm rad}\}$, where p_{y0} is the initial y momentum, and the last term denotes radiation reaction whose direction is opposite to the positron velocity. Figure 2(d) shows that the tracked positron first undergoes gyration motions in the first MFDR due to its low initial energy and then enters the EFDR for significant accelerations. As $E_y > B_z$ and small $P_{\rm rad}$ in these two regimes, the positron gains $p_y > 0$. After entering the second MFDR, the positron emits a high-energy photon and simultaneously its p_y is sharply decreased by radiation reaction (i.e., $P_{\rm rad}$ is large enough). As $E_y < B_z$ and $\beta_x > 0$ in the second MFDR, p_y gradually decreases and changes the sign to achieve $\theta_y < 0$. Here, the strong radiation of $\varepsilon_{\rm rad} > 0.2$ GeV is necessary for bunch-II positrons to flip their spins [54] and gain opposite deflection angles. This is supported by statistical results [Fig. 3(e)] that θ_y changes from positive to negative value as $\varepsilon_{\rm rad}$ increases. Note that bunch I finally obtains a small positive deflection angle $\bar{\theta}_y \approx 10^\circ$ in average, making less contribution to the overall polarization.

Therefore, under the joint action of spin flip and radiation reaction, positrons created in negative half cycles are generally polarized with $\bar{S}_z > 0$ at $\theta_y < 0$ and $\bar{S}_z < 0$ at $\theta_y > 0$ [Fig. 3(b)]. In positive half cycles, as the positron polarization at birth, and subsequent spin flip and deflection all rely on the direction of laser magnetic fields, the final polarization is still $\bar{S}_z > 0$ at $\theta_y < 0$ and $\bar{S}_z < 0$ at $\theta_y > 0$ [Fig. 3(h), with more details and a summary given by Fig. S8 and Table SI in SM]. The consistency of angle-dependent polarizations in all half cycles leads to the overall polarization as displayed in Fig. 1(c). The obtained electrons are also polarized like positrons, but with weaker polarization owing to the mixing of unpolarized target electrons (Fig. S7 in SM).

Parameter influences.—The dependence of positron yield N_+ and positron polarization $\bar{S}_z$ on the preplasma scale length L and laser amplitude a_0 are presented in Figs. 4(a) and 4(b), respectively. Preplasmas generated by laser prepulse are unavoidable and also adjustable in real experiments. Preplasmas of relatively low densities favor both N_+ and $\bar{S}_z$ by enhancing laser absorption and generating more ultrarelativistic electrons to trigger QED cascades [37]. The small scale length of $L = 0.4\mu$m leads to a significant laser reflection, where positrons are mainly created in strong standing waves away from the target surface [Fig. S9(a) in SM]. It implies that they would experience quasisymmetrical multicycle laser fields, detrimental to their polarizations. Excessive preplasmas of $L > 1.5$ μm also cause a slight decrease of $\bar{S}_z$ [Fig. 4(a)] since more laser energies are depleted by preplasmas before reaching the target bulk.

Positrons are polarized once the positron yield becomes appreciable with laser intensities above 10^{24} W cm^{-2} ($a_0 > 1000$). As shown in Fig. 4(b), N_+ increases with the growth of a_0, and $\bar{S}_z$ also tends to rise until a peak around $a_0 = 1700$. Low intensities cannot guarantee positron generation mainly near the target surface and strong photon emission [Fig. S9(b) in SM]. Similar trends are also observed for different target densities, but the optimized a_0 for peaked $\bar{S}_z$ decreases for a lower density [Fig. S10 in SM].

3D simulations.—Finally, 3D PIC simulations are conducted to validate the above 1D results. The incident laser has a transverse profile of $\exp[-(y^2 + z^2)/\sigma_0^2]$, with

$\sigma_0 = 2.0$ μm (a peak power of 197 PW). Other laser and target parameters are the same as Fig. 1. Figure 5(a) presents that positrons are composed of discrete bunches, consistent with Fig. 2(a). Similar angle-dependent polarization $\bar{S}_z$ can be observed in Fig. 5(b). The total positron yield is 550 nC; among them, around 30 nC positrons with a flux 10^{12} sr^{-1} acquire a polarization above 30%. Because of the tight focusing of laser fields, positrons are also slightly polarized in the y direction [Fig. 5(e)]. We find that the positron polarization is somewhat weaker when the laser is obliquely incident, and there are 22 nC positrons with the polarization above 30% for a 30° incidence angle (Fig. S11 in SM).

In conclusion, we have investigated dense polarized positrons and electrons from QED-dominated laser-solid interactions. About 30 nC transversely polarized positrons with the polarization degree above 30% can be generated at the laser intensity 3×10^{24} W/cm^2. Such high-charge and dense polarized positrons are promising for use in future electron-positron colliders via further wakefield accelerations [55–57], as well as to explore collective behavior of polarized plasmas [58,59]. The positron polarization mechanism is robust since the laser fields experienced by positrons are naturally asymmetric near the skin layer, and therefore polarized positrons could be ubiquitous in future 100-PW laser-solid experiments.

This work was supported by the National Key R&D Program of China (Grant No. 2018YFA0404801), National Natural Science Foundation of China (Grants No. 11775302 and No. 11827807), the Strategic Priority Research Program of Chinese Academy of Sciences (Grants No. XDA25050300 and No. XDA25010300), and the Fundamental Research Funds for the Central Universities, the Research Funds of Renmin University of China (20XNLG01).

*Corresponding author.
weiminwang1@ruc.edu.cn
†Corresponding author.
ytli@iphy.ac.cn

[1] G. Moortgat-Pick, T. Abe, G. Alexander, B. Ananthanarayan, A. Babich, V. Bharadwaj, D. Barber, A. Bartl, A. Brachmann, S. Chen *et al.*, Polarized positrons and electrons at the linear collider, Phys. Rep. **460**, 131 (2008).
[2] A. Vauth and J. List, Beam polarization at the ILC: Physics case and realization, Int. J. Mod. Phys. **40**, 1660003 (2016).
[3] D. W. Gidley, A. R. Köymen, and T. W. Capehart, Polarized Low-Energy Positrons: A New Probe of Surface Magnetism, Phys. Rev. Lett. **49**, 1779 (1982).
[4] C. Hugenschmidt, Positrons in surface physics, Surf. Sci. Rep. **71**, 547 (2016).
[5] A. K. Harding and D. Lai, Physics of strongly magnetized neutron stars, Rep. Prog. Phys. **69**, 2631 (2006).
[6] O. P. Novak and R. I. Kholodov, Spin-polarization effects in the processes of synchrotron radiation and electron-positron pair production by a photon in a magnetic field, Phys. Rev. D **80**, 025025 (2009).
[7] A. A. Sokolov and I. M. Ternov, *Synchrotron Radiation* (Akademie-Verlag, Berlin, 1968).
[8] V. N. Baier, Radiative polarization of electrons in storage rings, Sov. Phys. Usp. **14**, 695 (1972).
[9] G. Alexander *et al.*, Observation of Polarized Positrons from an Undulator-Based Source, Phys. Rev. Lett. **100**, 210801 (2008).
[10] T. Omori, M. Fukuda, T. Hirose, Y. Kurihara, R. Kuroda, M. Nomura, A. Ohashi, T. Okugi, K. Sakaue, T. Saito, J. Urakawa, M. Washio, and I. Yamazaki, Efficient Propagation of Polarization from Laser Photons to Positrons Through Compton Scattering and Electron-Positron Pair Creation, Phys. Rev. Lett. **96**, 114801 (2006).
[11] D. Abbott, P. Adderley, A. Adeyemi, P. Aguilera, M. Ali, H. Areti, M. Baylac, J. Benesch, G. Bosson, B. Cade *et al.* (PEPPo Collaboration), Production of Highly Polarized Positrons Using Polarized Electrons at MeV Energies, Phys. Rev. Lett. **116**, 214801 (2016).
[12] B. A. Remington, D. Arnett, R. P. Drake, and H. Takabe, Modeling astrophysical phenomena in the laboratory with intense lasers, Science **284**, 1488 (1999).
[13] B. A. Remington, R. P. Drake, and D. D. Ryutov, Experimental astrophysics with high power lasers and z pinches, Rev. Mod. Phys. **78**, 755 (2006).
[14] V. B. Berestetskii, E. M. Lifshitz, and L. P. Pitaevskii, *Quantum Electrodynamics* (Elsevier Butterworth-Heinemann, Oxford, 1982).
[15] V. N. Baier, V. Katkov, and V. M. Strakhovenko, *Electromagnetic Processes at High Energies in Oriented Single Crystals* (World Scientific, Singapore, 1998).
[16] V. I. Ritus, Quantum effects of the interaction of elementary particles with an intense electromagnetic field, J. Sov. Laser Res. **6**, 497 (1985).
[17] A. Di Piazza, C. Müller, K. Z. Hatsagortsyan, and C. H. Keitel, Extremely high-intensity laser interactions with fundamental quantum systems, Rev. Mod. Phys. **84**, 1177 (2012).
[18] A. Gonoskov, T. G. Blackburn, M. Marklund, and S. S. Bulanov, Charged particle motion and radiation in strong electromagnetic fields, arXiv:2107.02161.
[19] C. N. Danson, C. Haefner, J. Bromage, T. Butcher, J.-C. F. Chanteloup, E. A. Chowdhury, A. Galvanauskas, L. A. Gizzi, J. Hein, D. I. Hillier *et al.*, Petawatt and exawatt class lasers worldwide, High Power Laser Sci. Eng. **7**, e54 (2019).
[20] J. W. Yoon, Y. G. Kim, I. W. Choi, J. H. Sung, H. W. Lee, S. K. Lee, and C. H. Nam, Realization of laser intensity over 10^{23} W/cm^2, Optica **8**, 630 (2021).
[21] Extreme Light Infrastructure (ELI), https://eli-laser.eu.
[22] E. Cartlidge, The light fantastic, Science **359**, 382 (2018).
[23] B. Shao, Y. Li, Y. Peng, P. Wang, J. Qian, Y. Leng, and R. Li, Broad-bandwidth high-temporal-contrast carrier-envelope-phase-stabilized laser seed for 100 PW lasers, Opt. Lett. **45**, 2215 (2020).
[24] Exawatt Center for Extreme Light Studies (XCELS), https://xcels.iapras.ru.
[25] E. Cartlidge, Eastern Europe's laser centers will debut without a star, Science **355**, 785 (2017).

[26] H. R. Reiss, Absorption of light by light, J. Math. Phys. (N.Y.) **3**, 59 (1962).
[27] I. V. Sokolov, N. M. Naumova, J. A. Nees, and G. A. Mourou, Pair Creation in QED-Strong Pulsed Laser Fields Interacting with Electron Beams, Phys. Rev. Lett. **105**, 195005 (2010).
[28] T. G. Blackburn, A. Ilderton, C. D. Murphy, and M. Marklund, Scaling laws for positron production in laser–electron-beam collisions, Phys. Rev. A **96**, 022128 (2017).
[29] F. Wan, R. Shaisultanov, Y.-F. Li, K. Z. Hatsagortsyan, C. H. Keitel, and J.-X. Li, Ultrarelativistic polarized positron jets via collision of electron and ultraintense laser beams, Phys. Lett. B **800**, 135120 (2020).
[30] Y.-Y. Chen, P.-L. He, R. Shaisultanov, K. Z. Hatsagortsyan, and C. H. Keitel, Polarized Positron Beams via Intense Two-Color Laser Pulses, Phys. Rev. Lett. **123**, 174801 (2019).
[31] A.-C. Tien, S. Backus, H. Kapteyn, M. Murnane, and G. Mourou, Short-Pulse Laser Damage in Transparent Materials as a Function of Pulse Duration, Phys. Rev. Lett. **82**, 3883 (1999).
[32] E. N. Nerush, I. Y. Kostyukov, A. M. Fedotov, N. B. Narozhny, N. V. Elkina, and H. Ruhl, Laser Field Absorption in Self-Generated Electron-Positron Pair Plasma, Phys. Rev. Lett. **106**, 035001 (2011).
[33] X.-L. Zhu, T.-P. Yu, Z.-M. Sheng, Y. Yin, I. C. E. Turcu, and A. Pukhov, Dense GeV electron-positron pairs generated by lasers in near-critical-density plasmas, Nat. Commun. **7**, 13686 (2016).
[34] T. Grismayer, M. Vranic, J. L. Martins, R. A. Fonseca, and L. O. Silva, Seeded QED cascades in counterpropagating laser pulses, Phys. Rev. E **95**, 023210 (2017).
[35] C. P. Ridgers, C. S. Brady, R. Duclous, J. G. Kirk, K. Bennett, T. D. Arber, A. P. L. Robinson, and A. R. Bell, Dense Electron-Positron Plasmas and Ultraintense γ Rays from Laser-Irradiated Solids, Phys. Rev. Lett. **108**, 165006 (2012).
[36] I. Y. Kostyukov and E. N. Nerush, Production and dynamics of positrons in ultrahigh intensity laser-foil interactions, Phys. Plasmas **23**, 093119 (2016).
[37] W.-M. Wang, P. Gibbon, Z.-M. Sheng, Y.-T. Li, and J. Zhang, Laser opacity in underdense preplasma of solid targets due to quantum electrodynamics effects, Phys. Rev. E **96**, 013201 (2017).
[38] N. V. Elkina, A. M. Fedotov, I. Y. Kostyukov, M. V. Legkov, N. B. Narozhny, E. N. Nerush, and H. Ruhl, QED cascades induced by circularly polarized laser fields, Phys. Rev. ST Accel. Beams **14**, 054401 (2011).
[39] C. Ridgers, J. Kirk, R. Duclous, T. Blackburn, C. Brady, K. Bennett, T. Arber, and A. Bell, Modelling gamma-ray photon emission and pair production in high-intensity laser-matter interactions, J. Comput. Phys. **260**, 273 (2014).
[40] A. Gonoskov, S. Bastrakov, E. Efimenko, A. Ilderton, M. Marklund, I. Meyerov, A. Muraviev, A. Sergeev, I. Surmin, and E. Wallin, Extended particle-in-cell schemes for physics in ultrastrong laser fields: Review and developments, Phys. Rev. E **92**, 023305 (2015).
[41] H.-H. Song, W.-M. Wang, and Y.-T. Li, YUNIC: A multi-dimensional particle-in-cell code for laser-plasma interaction, arXiv:2104.00642.
[42] H.-H. Song, W.-M. Wang, Y.-F. Li, B.-J. Li, Y.-T. Li, Z.-M. Sheng, L.-M. Chen, and J. Zhang, Spin and polarization effects on the nonlinear Breit-Wheeler pair production in laser-plasma interaction, New J. Phys. **23**, 075005 (2021).
[43] A. Macchi, M. Borghesi, and M. Passoni, Ion acceleration by superintense laser-plasma interaction, Rev. Mod. Phys. **85**, 751 (2013).
[44] Y.-F. Li, Y.-Y. Chen, W.-M. Wang, and H.-S. Hu, Production of Highly Polarized Positron Beams via Helicity Transfer from Polarized Electrons in a Strong Laser Field, Phys. Rev. Lett. **125**, 044802 (2020).
[45] Y.-F. Li, R. Shaisultanov, Y.-Y. Chen, F. Wan, K. Z. Hatsagortsyan, C. H. Keitel, and J.-X. Li, Polarized Ultrashort Brilliant Multi-GeV γ Rays via Single-Shot Laser-Electron Interaction, Phys. Rev. Lett. **124**, 014801 (2020).
[46] K. Yokoya, User's Manual of CAIN Version 2.42 (2011).
[47] See Supplemental Material at http://link.aps.org/supplemental/10.1103/PhysRevLett.129.035001 for detailed simulation methods and additional simulation results, which includes Refs. [48–50].
[48] W. H. McMaster, Matrix representation of polarization, Rev. Mod. Phys. **33**, 8 (1961).
[49] Y. Tang, Z. Gong, J. Yu, Y. Shou, and X. Yan, Radiative polarization dynamics of relativistic electrons in an intense electromagnetic field, Phys. Rev. A **103**, 042807 (2021).
[50] V. Bargmann, L. Michel, and V. L. Telegdi, Precession of the Polarization of Particles Moving in a Homogeneous Electromagnetic Field, Phys. Rev. Lett. **2**, 435 (1959).
[51] P. Gibbon, *Short Pulse Laser Interactions with Matter: An Introduction* (Imperial College Press, London, 2005).
[52] V. F. Bashmakov, E. N. Nerush, I. Y. Kostyukov, A. M. Fedotov, and N. B. Narozhny, Effect of laser polarization on quantum electrodynamical cascading, Phys. Plasmas **21**, 013105 (2014).
[53] T. Z. Esirkepov, S. S. Bulanov, J. K. Koga, M. Kando, K. Kondo, N. N. Rosanov, G. Korn, and S. V. Bulanov, Attractors and chaos of electron dynamics in electromagnetic standing waves, Phys. Lett. A **379**, 2044 (2015).
[54] H.-H. Song, W.-M. Wang, J.-X. Li, Y.-F. Li, and Y.-T. Li, Spin-polarization effects of an ultrarelativistic electron beam in an ultraintense two-color laser pulse, Phys. Rev. A **100**, 033407 (2019).
[55] S. Zhou, J. Hua, W. An, W. B. Mori, C. Joshi, J. Gao, and W. Lu, High Efficiency Uniform Wakefield Acceleration of a Positron Beam Using Stable Asymmetric Mode in a Hollow Channel Plasma, Phys. Rev. Lett. **127**, 174801 (2021).
[56] T. Silva, L. D. Amorim, M. C. Downer, M. J. Hogan, V. Yakimenko, R. Zgadzaj, and J. Vieira, Stable Positron Acceleration in Thin, Warm, Hollow Plasma Channels, Phys. Rev. Lett. **127**, 104801 (2021).
[57] W.-Y. Liu, K. Xue, F. Wan, M. Chen, J.-X. Li, F. Liu, S.-M. Weng, Z.-M. Sheng, and J. Zhang, Trapping and acceleration of spin-polarized positrons from γ photon splitting in wakefields, Phys. Rev. Research **4**, L022028 (2022).
[58] M. Marklund and G. Brodin, Dynamics of Spin-$\frac{1}{2}$ Quantum Plasmas, Phys. Rev. Lett. **98**, 025001 (2007).
[59] G. Brodin and M. Marklund, Spin solitons in magnetized pair plasmas, Phys. Plasmas **14**, 112107 (2007).